How to cite: Angew. Chem. Int. Ed. 2023, e202315280
doi.org/10.1002/anie.202315280

VIP Metal-Organic Frameworks Very Important Paper

Zr-Porphyrin Metal–Organic Framework as nanoreactor for boosting the formation of hydrogen clathrates

Carolina Carrillo-Carrión, Judit Farrando-Perez, Luke L. Daemen, Yongqiang Q. Cheng, Anibal J. Ramirez-Cuesta, and Joaquin Silvestre-Albero**

Abstract: We report the first experimental evidence for rapid formation of hydrogen clathrates under mild pressure and temperature conditions within the cavities of a zirconium-metalloporphyrin framework, specifically PCN-222. PCN-222 has been selected for its 1D mesoporous channels, high water-stability, and proper hydrophilic behavior. Firstly, we optimize a microwave (MW)-assisted method for the synthesis of nanosized PCN-222 particles with precise structure control (exceptional homogeneity in morphology and crystalline phase purity), taking advantage of MW in terms of rapid/homogeneous heating, time and energy savings, as well as potential scalability of the synthetic method. Second, we explore the relevance of the large mesoporous 1D open channels within the PCN-222 to promote the nucleation and growth of confined hydrogen clathrates. Experimental results show that PCN-222 drives the nucleation process at a lower pressure than the bulk system (1.35 kbar vs 2 kbar), with fast kinetics (minutes), using pure water, and with a nearly complete water-to-hydrate conversion. Unfortunately, PCN-222 cannot withstand these high pressures, which lead to a significant alteration of the mesoporous structure while the microporous network remains mainly unchanged.

Introduction

Clathrate hydrates are crystalline solids formed in nature when water and gas molecules are in contact under favorable pressure and temperature conditions.[1] Clathrate hydrates are considered the main reservoir for gases on Earth. Natural clathrate hydrates are located either at the seabed (marine sediments) or in the permafrost.[1–3] Despite their abundance in nature, clathrate hydrates are usually associated with guest molecules above 0.33–0.36 nm (e.g., CO_2, Ar, and N_2) due to the necessity to stabilize the 3D network. This assumption was rebutted by Vos et al. in 1993 using high-pressure optical and X-ray studies of H_2-H_2O mixtures.[4] These authors proved the successful incorporation of H_2 molecules in the voids of H_2O frameworks, albeit at high pressure conditions (pressure range 7.5–31.0 kbar). The first conclusive evidence of hydrogen clathrate hydrate formation dates back to 2002. Mao et al. managed to enclathrate hydrogen molecules in the cages of hydrogen bonded water molecules in an sII crystal structure.[2] High-pressure Raman, infrared, X-ray, and neutron studies allowed to prove *for the first time* the presence of multiple occupancy in hydrate cages, with four H_2 molecules in the large cages ($5^{12}6^4$) and two hydrogen molecules in the small cages (5^{12}), thus giving rise to a stoichiometry of $64H_2 \cdot 136H_2O$. Due to the small kinetic diameter of hydrogen (0.272 nm), pressures above 2 kbar using a diamond anvil cell (DAC) at 300 K were required to promote the formation of these crystalline structures on a small scale. Taking inspiration from nature, Mao et al. opened the gate to consider clathrate hydrates as potential reservoirs for hydrogen storage with a maximum capacity (considering the full occupation of cages) of ca. 5.0 wt % and 46.7 g/L.

Despite the promising results achieved so far, two critical drawbacks require further investigations for a potential application, namely (i) the high pressure needed to initiate the nucleation process, and (ii) the slow formation kinetics, due to the limited gas-liquid interface in bulk conditions. Incorporation of a second guest component (THF) was proposed by Floresee et al. to stabilize clusters of H_2 clathrate hydrate at lower pressures.[5] Taking advantage of the stabilizing properties of THF, these binary clathrate hydrates could be synthesized at pressures around 0.05 kbar and 280 K. However, the partial occupation of the large cages by THF limited the total amount of hydrogen stored (ca. 2.1 wt %).[5,6] Smaller concentrations of THF (0.1 mol %) allowed to place H_2 molecules in the large cages at 0.12 kbar, the gravimetric capacity rising to ca. 4 wt %.[6]

[*] J. Farrando-Perez, J. Silvestre-Albero
Laboratorio de Materiales Avanzados, Departamento de Química Inorgánica-Instituto Universitario de Materiales, Universidad de Alicante
03690 San Vicente del Raspeig (Spain)
E-mail: joaquin.silvestre@ua.es

C. Carrillo-Carrión
Institute for Chemical Research (IIQ), CSIC – University of Seville
41092 Seville (Spain)
E-mail: carolina.carrillo@csic.es

L. L. Daemen, Y. Q. Cheng, A. J. Ramirez-Cuesta
Spallation Neutron Source, Oak Ridge National Laboratory
Oak Ridge, TN 37831 (USA)

However, the reaction was too slow to make it practical. Recent studies have indicated that activated carbon materials with a perfectly tailored porous structure and surface chemistry can promote the nucleation and growth of H_2 clathrate hydrates using pure water at lower pressures than the bulk system (1.35 vs 2.0 kbar).[7] Thanks to confinement effects, massive hydrogen hydrates were obtained with a nearly complete water-to-hydrate conversion, and with very fast kinetics.

Encouraged by those successful results, we sought to investigate if this hypothesis (proof-of-concept) could also be extended to metal–organic frameworks (MOFs), given their superior properties compared to conventional porous material such as: (i) higher structural and chemical tunability: the proper selection of the inorganic/metal nodes and organic linkers allows the rational design of the MOF's structure, and therefore its physicochemical features in terms of pore size (ranging from micro- to mesopores), hydrophobic/hydrophilic character, and functional organic groups (to further establish different chemical/bonding interactions with guest molecules); and (ii) easy of post-synthetic modification (PSM) strategies in MOFs (both in the external surface and internal pore space) to finely modulate specific interactions with the desired guest molecules and/or to stabilize the in situ formed species (or trapped species) inside their ordered and regular cavities. Compared to carbon materials, MOFs can be prepared using a wide variety of metallic centers and organic linkers, thus giving rise to purpose-designed structures with defined pore dimensions and surface chemistry for the efficient adsorption of H_2 and/or the stabilization of the formed species though specific interactions. In this sense, MOFs are promising candidates to widen the possibilities to design porous structures to promote the nucleation and growth of gas hydrates under confinement. Furthermore, thanks to their crystalline nature, with atoms uniformly located at specific sites along the framework, MOFs have uniform cavities (i.e., pores with the same coordination environment and, therefore, with identical adsorption properties and reactivity) which in turns will allow a better control of their performance as "nanoreactors" to carry out controlled chemical reactions, and/or growth of other target structures/species. Based on previous studies for methane hydrate clathrate in the confined nanospace of MOFs,[8,9] a mesoporous MOF with a proper hydrophilic character and water stability, such as the zirconium-metalloporphyrin PCN-222 has been selected as the target host structure. PCN-222 (also known as MOF-545) consists of Zr_6 clusters with eight edges connected to the square planar tetrakis(4-carboxyphenyl)porphyrin (TCPP) linkers giving rise to a 3D network with Kagome-like topology (Figure 1A), and featuring two types of cavities: triangular 1D channels with a diameter of 1.7 nm (microporous) and very large hexagonal 1D open channels with a diameter as large as 3.7 nm (mesoporous) along the *c* axis, a size which is among one of the largest reported in MOFs.[10]

It is worth to note that to exploit the full potential of MOFs in many applications (as the one proposed in this work), a precise control of the MOF synthesis is a must; this is the only way to ensure the correct interpretation of the results, avoiding misunderstandings due to material inhomogeneities, as well as to achieve a good batch-to-batch reproducibility, which is also a critical issue for the further transfer of the developed MOF-based methodology to real scenarios. The latter implies that the cost and potential scalability of the MOF synthesis must be considered. With these considerations in mind, we have optimized the synthesis of nanosized PCN-222 under microwave (MW) irradiation. The expected positive effect of MW on the MOF's synthesis is attributed to the particular way of heating, i.e., volumetric heating, which is different from conventional heating.[11] This translates into several advantages such as: (i) more homogeneous temperature profile, resulting in more homogeneous particles (high monodispersity); (ii) fast heating and reduction of the activation barrier energy, thereby increasing the nucleation rate, and allowing thus smaller particle sizes and high crystalline phase-selectivity; (iii) reduction of synthesis time from hours or days to only a few minutes, with consequent energy savings; (iv) higher yields and easier to scale-up compared to conventional solvothermal reactions. Surprisingly, only a few types of MOFs have been successfully prepared by MW to date,[12,13] and these reported examples rarely achieved nanoMOFs with a good control in the particle homogeneity.

Results and Discussion

After a careful optimization process of the MW method, we succeeded in preparing high-quality rod-shaped PCN-222 nanoparticles with an average length of ca. 200 nm by mixing TCPP (22.5 mg, 28.5 μmol), Zr_6 clusters (38 mg, 14.2 μmol) and trifluoroacetic acid (TFA, 160 μL), previously dissolved in dry DMF (16 mL), and heating this mixture at 393 K for 10 min under MW irradiation (initial power 200 W; the fixed temperature of 393 K is reached in 60 s, and power is then stabilized at 60 W; no pressure is applied). After this time the reaction mixture became turbid (red-purple in color), indicative of the formation of the solid PCN-222 particles, which were further purified and activated (see Supporting Information for details; Scheme S1). It is worth noting that the use of pre-formed Zr_6 clusters as zirconium source (instead of $ZrCl_4$) and trifluoroacetic acid (TFA) as a modulator agent are key points for achieving nanosized PCN-222 particles with pure crystalline phase, as recently reported by Fairen et al.[14] In addition, continuous stirring (600 rpm) during the synthesis and subsequent rapid cooling were found to be important factors in the homogeneity of the obtained nanoparticles. We also found that the particle size could be readily modulated by simply changing the concentration of the precursors (TCPP and Zr_6 nodes) in the reaction mixture; doubling the concentration but keeping the TCPP/Zr_6 ratio constant produced an increase in size from ca. 200 nm to 500 nm (Figure S1, see Supporting Information for details). In general, the reduction of the particle size allows for a faster diffusion of the guest molecules towards the internal void space and is therefore preferred. However, very small particles are also less stable

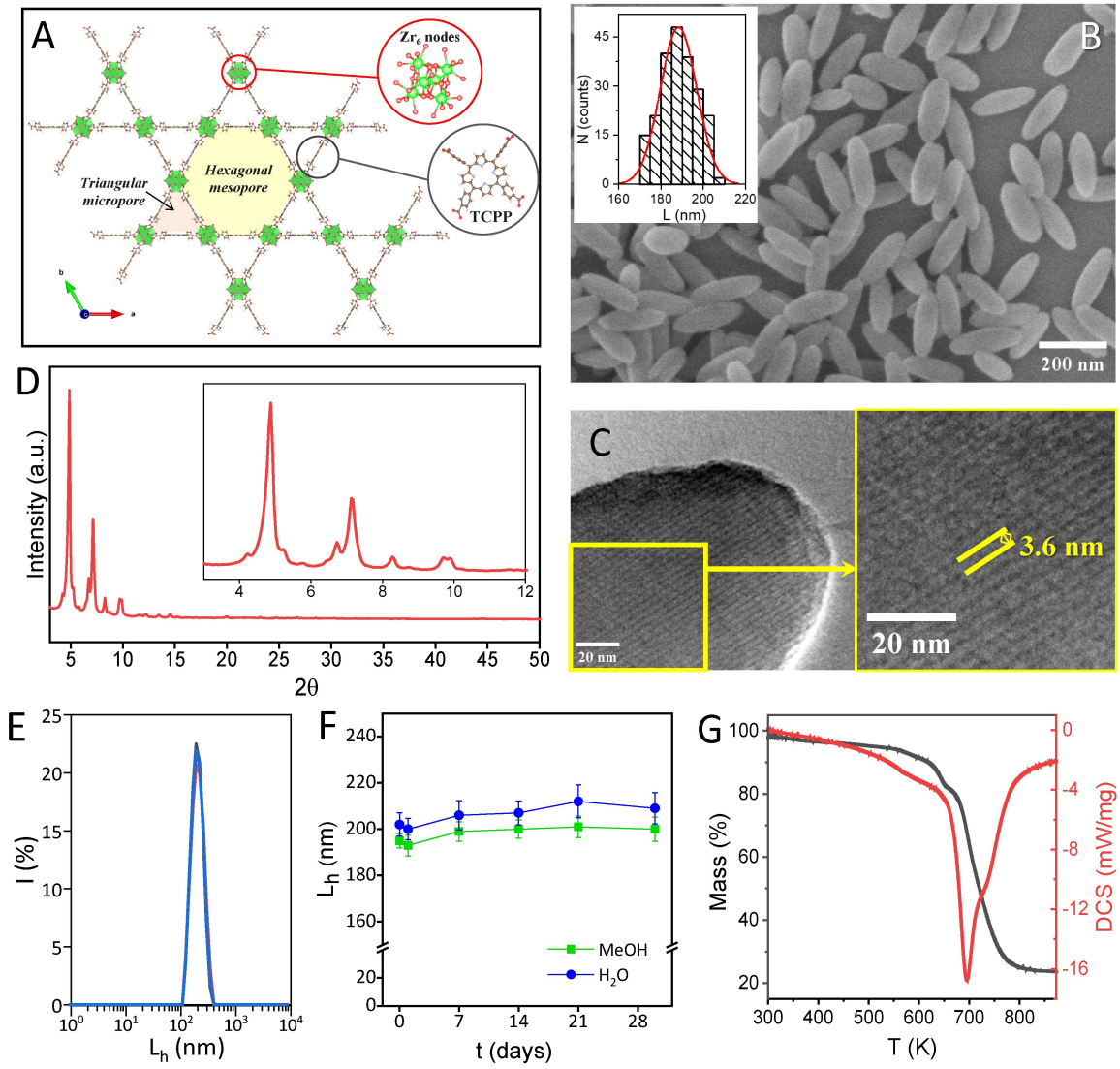

Figure 1. (A) 3D structure of PCN-222 viewed along the c-axis to show the two types of 1D open channels. PCN-222 is formed by TCPP linkers attached to four 8-connected Zr_6 clusters (building units shown in circles). (B) SEM image of the as-prepared PCN-222 particles under MW irradiation. Inset: Histogram of the number distribution of the length of the particles as determined from SEM images; average length $L = 188 \pm 10$ nm. (C) HRTEM image of a PCN-222 particle, revealing the existence of highly oriented mesopores. (D) PXRD pattern of the PCN-222 nanoparticles, showing magnification within the range $2\theta = 3°–12°$ (inset). (E) DLS size distributions by intensity of the particles dispersed in methanol ($n = 3$, mean hydrodynamic length of $L_b = 195 \pm 3$ nm). (F) Colloidal stability over time of the particles dispersed in either methanol or water, as determined by DLS. (G) TGA and DSC curves of the PCN-222 recorded in a dynamic air atmosphere.

under harsh conditions over an extended period of time, and a compromise needs to be found. To this effect, we chose PCN-222 with an average length of 188 ± 10 nm as determined by scanning and transmission electron microscopy (SEM and TEM; Figure 1B and Figure S2), and in which the short intracrystalline diffusional paths should facilitate the diffusion of H_2 throughout the PCN-222 particle. SEM and TEM images also showed the good uniformity (in size and shape) of the as-synthesized particles, whereas high-resolution TEM (HRTEM) revealed the existence of highly oriented longitudinal mesopores (Figure 1C). Powder X-ray diffraction (PXRD) revealed the high crystallinity of the as-prepared PCN-222 nanoparticles (Figure 1D), which agrees with the simulated pattern predicted from the single-crystal structure,[14] which confirmed the phase purity of our PCN-222 material.

Regarding the practical aspects of the optimized synthetic method, we should remark that the PCN-222 particles were prepared in only 10 min, a considerably shorter time than that required in conventional solvothermal methods (e.g., 5 h by using a block heater at 393 K).[14] This highlights one of the most advantageous features of using the MW technology in the synthesis of MOFs. Besides, the use of TFA as the modulator instead of benzoic acid (the most common modulator in the synthesis of Zr-based MOFs) simplified the synthesis, specifically the purification and activation steps. Several washes with DMF and methanol were enough to completely eliminate the TFA. Treatment

with concentrated HCl, as the typical activation step to remove the trapped benzoic acid and recover the MOF porosity is not needed. ^{19}F nuclear magnetic resonance (NMR) spectroscopy of the digested PCN-222 sample (digestion in 0.1 M NaOH in D_2O) was used to check the removal of TFA in the purified PCN-222. No detectable TFA peak was found in the digested PCN-222 sample, whereas the intentional addition of TFA traces showed the corresponding signal at δ -75.5 ppm (Figure S3). In addition to these advantageous aspects of the synthesis, the batch-to-batch reproducibility was surprisingly good; a critical feature that is quite often overlooked (Figure S4).

Dynamic light scattering (DLS) measurements in solution showed a hydrodynamic size slightly larger ($L_h = 195 \pm 3$ nm, Figure 1E, Figure S5 and Table S2) than the length of the dried particles determined by SEM. This was expected due to the solvation layer around the particles. Importantly, the polydispersity index was quite low (PdI = 0.065), indicative of the exceptional homogeneity of the particles and lack of aggregation. We also investigated the colloidal stability over time of the PCN-222 dispersed in either methanol or water by monitoring the L_h of the particles in solution over a period of one month. As shown in Figure 1F the changes in L_h were negligible, reflecting the good colloidal stability of the particles in both media (Table S3). PCN-222 also presented a high thermal stability in air up to 617 K, as indicated by the thermogravimetric analysis (TGA) data (Figure 1G). All these characterization data confirmed that we have successfully developed an efficient, simple, and fast MW-assisted method for the synthesis of nanosized and highly uniform PCN-222 particles.

The porosity of the as-synthetized PCN-222 nanoparticles was also determined. The Brunauer–Emmett–Teller (BET) area was determined to be 1885 $m^2 g^{-1}$ and the total pore volume was 1.50 $cm^3 g^{-1}$. The N_2 adsorption-desorption curves (Figure 2A) obtained at 77 K exhibited a combination of type I and type IV isotherms, according to the IUPAC classification, showing two steep increases at the points of $P/P_0 = 0.05$ (micropore filling) and 0.3 (mesopore condensation), respectively, indicating the presence of both micropores and mesopores within the PCN-222 particles. The mesopore volume was calculated to be 55 % of the total volume (Table S1). In addition, the mesopore size along the *c*-axis was calculated to be 3.6 nm, as derived from pore size distribution obtained after application of the non-local density functional theory (NLDFT) to the N_2 adsorption data (Figure 2B). The estimated pore size fits quite well with the theoretical size (3.7 nm), and also with the estimated value from HRTEM images (Figure 1C). Closer inspection of the shape of the hysteresis loop (type H1 as defined by IUPAC)[15] disclosed the existence of well-defined cylindrical-like pore channels.[16] After determination of the pore characteristics, we turned our attention to the water adsorption properties of the as-synthetized particles. H_2O adsorption/desorption isotherms are essential to identify the location of the water molecules (adsorption sites) and the suitability of PCN-222 as a material to host confined gas clathrates. The H_2O isotherms at 298 K (Figure 2C) showed the characteristic behavior of a material with a poor water-framework interaction (type IV isotherm), and thus with a limited amount adsorbed up to $P/P_0 \approx 0.7$. Above this threshold pressure, the isotherm exhibited a sharp increase in the amount of water adsorbed. This increase is associated with the capillary condensation of H_2O molecules in the inner cavities of the MOF (mainly water condensation in mesocavities). The total amount adsorbed at saturation reached ca. 49 mmol/g (i.e., 0.88 mL/g, in close agreement with the mesopore volume obtained from the N_2 adsorption data). However, the participation of the micropores in the H_2O adsorption process, assisted by mesopores, cannot be ruled out. The desorption branch exhibited two well-defined regions with a sharp desorption at $P/P_0 \approx 0.6$, followed by a progressive decay to a steady state below $P/P_0 \approx 0.4$. These two regions could be associated with the massive emptying of the mesopores (first step), followed by the removal of H_2O molecules directly interacting with the MOF framework, i.e., organic linkers (second step). The presence of a marked hysteresis loop down to low relative pressures suggests the presence of H_2O molecules strongly interacting with the MOF framework, most probably due to their irreversible bonding to Zr-clusters.[17] Highly hydrophilic or hydrophobic behavior in MOFs is detrimental to the nucleation and growth of gas hydrates in their confined environment.[9] In this respect, the appropriate hydrophobic/

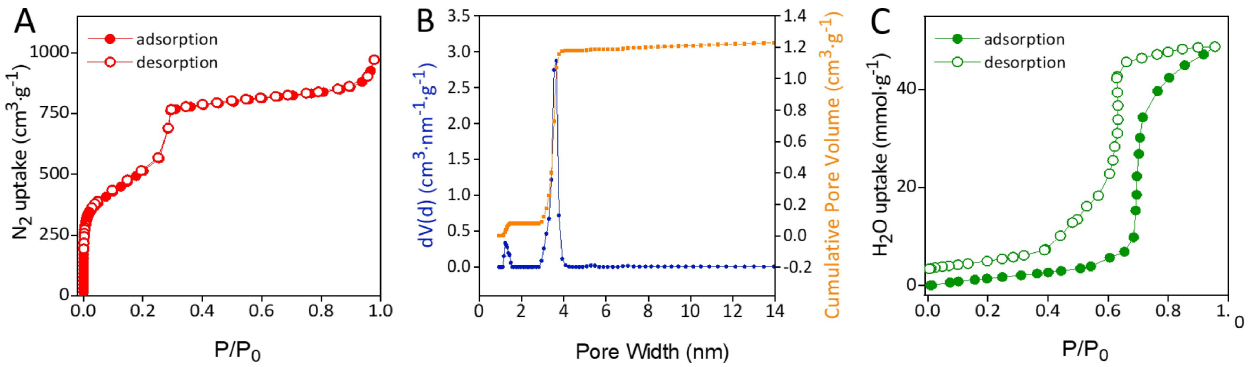

Figure 2. (A) N_2 isotherms (77 K) of the as-synthesized PCN-222 particles, and (B) corresponding NLDFT pore size distribution analysis. (C) H_2O isotherms (298 K) of the as-synthesized PCN-222.

hydrophilic balance observed in PCN-222, combined with the large adsorption capacity at saturation (due to the wetting of the inner cavities) represents, a priori, a promising scenario to promote the nucleation and growth of confined hydrates crystals.

With these nanoparticles at hand, we sought to explore their potential as nanoreactors for boosting the formation of hydrogen clathrates under mild conditions. To ascertain the possible formation of hydrogen clathrate hydrates, the PCN-222 sample was loaded with D_2O to the amount needed to fill completely the porosity (1.5–1.6 mL/g, based on the total pore volume obtained from the N_2 adsorption data). Once pre-impregnated, the sample was pressurized with pure hydrogen at 1.35 kbar, 1.65 kbar and 2.0 kbar and 280 K for 30 minutes using specially designed CuBe pressure cells. After pressurization, the samples were cooled down to 5 K to carry out inelastic neutron scattering (INS) measurements. To prevent solid hydrogen formation, the pressure cell was evacuated down to atmospheric pressure upon reaching a temperature of 160 K. Figure 3A shows the INS scattering spectrum in the low energy transfer region for the PCN-222 sample pressurized at the three pressures mentioned above. The INS spectrum of the sample pressurized at 1.35 kbar was dominated by two broad contributions at around 7.5–12 meV and 12.5–16 meV. The second contribution clearly reflects the rotational line of parahydrogen. This contribution has been widely investigated in the literature with the maximum traditionally being reported at 14.7 meV for the free rotor.[18] The first band was broader and contained two contributions at around 8 and 10 meV. This doublet is assigned to the orthohydrogen vibrational transitions due to the entrapment of hydrogen in the clathrate cages.[7] These results confirm that, as predicted, PCN-222 seems to be a good host to boost the nucleation and growth of hydrogen clathrate hydrates at a lower pressure than the bulk system (1.35 vs 2.0 kbar) and with fast kinetics (the stabilization time at 280 K is only 30 min, whereas the cooling process to 160 K takes 2 h). To further evaluate the effect of the formation pressure, PCN-222 loaded with D_2O was pressurized with hydrogen at 1.65 kbar and 2.0 kbar. Despite using more favorable experimental conditions for clathrate formation, the INS spectral features due to enclathrated hydrogen decreased in intensity, this effect being more significant at 2.0 kbar. Apparently, hydrogen clathrate hydrates were promoted at low pressures while seemingly more favorable conditions inhibited the ice-to-hydrate conversion.

To further understand the nucleation processes taking place in the presence of PCN-222, the neutron diffraction (ND) signal measured at VISION was evaluated. Figure 3B shows the diffraction patterns for the sample loaded with D_2O, in the absence of hydrogen pressure, and after pressurization at 1.35, 1.65 and 2.0 kbar. The ND pattern of PCN-222 loaded with D_2O at 5 K showed the characteristic peaks of hexagonal ice at 3.4 Å, 3.6 Å and 3.9 Å. More specifically, these peaks correspond to the (100), (002) and (101) planes in ice Ih. Despite the perfect matching in peak position with the theoretical ND pattern of hexagonal ice, there is an important discrepancy in the relative intensity of the different peaks. Compared to solid ice, the (100) and (101) peaks in confined D_2O are much weaker relative to the (002) peak. This observation clearly reflects the presence of defective ice structures, most probably due to the confinement of D_2O in the unidirectional mesoporous channels of PCN-222. As a result of this confinement, the stacking sequence of the hexagonal layers is disordered, although the interlayer distance is well preserved, i.e., stacking-disordered ice. Interestingly, the scenario changed drastically at 1.35 kbar. In agreement with INS measurements, the ND peaks due to hexagonal ice vanished completely and new peaks appeared at 3.0 Å, 3.2 Å, 4.9 Å and 5.1 Å, characteristic of the sII structure of hydrogen clathrate hydrates. The

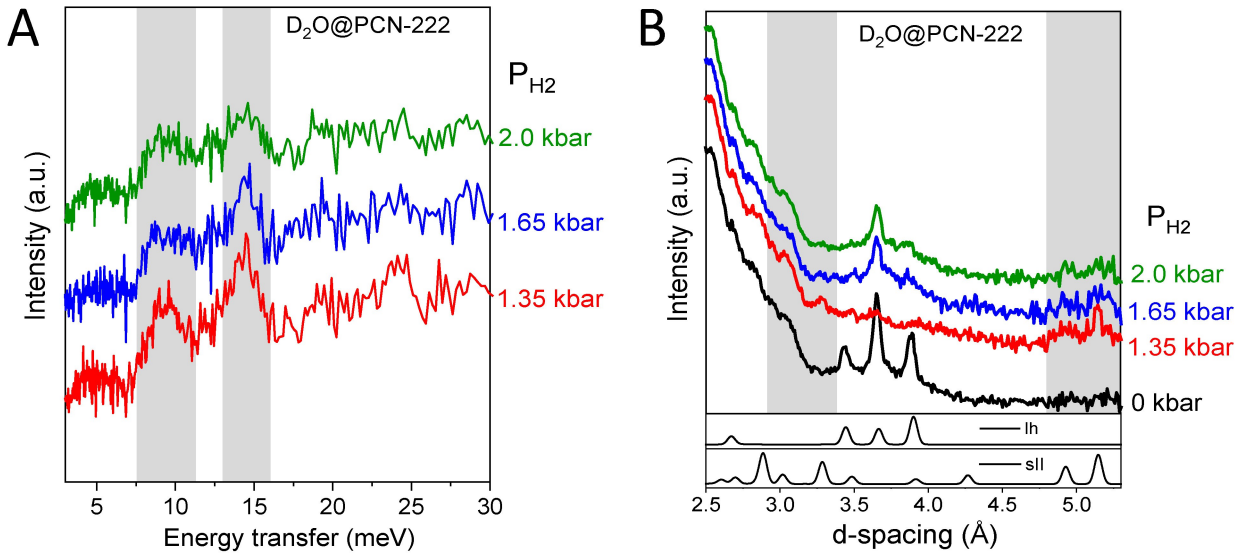

Figure 3. (A) INS spectra, and (B) ND patterns at 5 K for D_2O impregnated PCN-222 after pressurization with hydrogen at three different pressures, 1.35 kbar, 1.65 kbar and 2.0 kbar. ND pattern in the absence of hydrogen as control is also shown.

absence of any peak attributed to hexagonal ice reflects the nearly complete water-to-hydrate conversion. This result constitutes the first experimental evidence for hydrogen clathrate hydrate formation in MOFs, and provide a clear proof regarding the potential of PCN-222 to act as a nanoreactor to promote the nucleation and growth of these confined crystals. Given the unit cell parameter ($a = 17.083 \pm 0.018$ Å), hydrogen clathrate hydrates formation must take place preferentially in the highly-extended longitudinal mesoporous cavities in PCN-222, i.e., participation of micropores present in PCN-222 can be ruled out due to size limitations, at least to accommodate stoichiometric clathrates.[2,8] Unexpectedly, a further increase in the hydrogen pressure to 1.65 kbar and 2.0 kbar proved detrimental for the clathrate formation process. The hydrogen clathrate hydrate peaks disappeared and a new peak at 3.6 Å dominates the pattern. Although this contribution fits the (002) diffraction peak of hexagonal ice, the absence of the (100) and (101) peaks clearly indicates the presence of a highly defective ice phase in the confined environment of the unidirectional channels of PCN-222, thus confirming the INS results. The XRD pattern presented some similarities with a metastable cubic ice structure (ice Ic), but must be rather composed of randomly stacked defective layers of cubic and hexagonal sequences (vein-like entrapped D_2O molecules).[19] This kind of disorders are common in mesoporous silica materials, such as SBA-15 and KIT-6.[20]

As previously mentioned, the absence of water-to-hydrate conversion at higher hydrogen pressures is unexpected despite the favorable P–T conditions. Previous studies have shown that PCN-222 is a highly flexible MOF under variable temperature conditions.[21] It is commonly observed in mesoporous MOFs that enlarged pore sizes weaken the framework stability when the material is subjected to harsh conditions.[22] Although there are no data in the literature about the performance of PCN-222 under these extreme pressure conditions, it is also well-known that MOFs respond to pressure with a wide range of potential structural changes (phase transition, amorphization, distortion of the crystal structure with possible associated loss of symmetry, etc.).[23]

To ascertain potential structural changes in PCN-222 after the hydrogen clathrate hydrate formation process, the recovered sample was further characterized using PXRD, N_2 isotherms and TEM. Figure 4A compares the PXRD pattern of PCN-222 for the original and used samples, i.e., before and after the formation of clathrates. There is a significant broadening of the main diffraction peaks at low angles (4.9° and 7.0°), corresponding to the (200) and (201) planes. However, the absence of shifts in these two Bragg peaks, which fit perfectly with the hexagonal space group P6/mmm, seems to indicate that a phase transition did not occur. The broadening of XRD peaks indicates that either the clathrate formation or the application of high pressure, made the crystal lattice become imperfect. Deviations from an ideal crystalline lattice (i.e., perfectly ordered crystalline array) could explain our observations: partial amorphization (not total since the material was still crystalline) or defect creation (e.g., linker vacancies under pressure). Since the PXRD measurement was performed with the recovered sample after pressure release (ex situ), these observations point out that the structural alterations in PCN-222 are irreversible, i.e., the long-range ordering is not recovered after returning to ambient conditions.[24] Similarly, N_2 uptake data at 77 K in the recovered sample revealed a significant decrease in the accessible surface area (BET area ca. 1295 $m^2 g^{-1}$, Figure 4B and Table S4). Surprisingly, while the microporous structure was largely preserved (except some enhanced N_2 adsorption at very low relative pressures (Figure S6), probably due to a small shrinkage of the microporous structure), the mesoporosity was significantly affected, as demonstrated by an important decrease in the mesopore volume (Table S4 and Figure 4C). These findings could suggest either a blocking of the mesopores by D_2O molecules trapped after the gas hydrate formation process or to the alteration of the 3D structure of the MOF upon the clathrate formation process under high pressure conditions. Farha et al. reported that for the dehydration of NU-1000, another Zr-MOF that contained the same Zr_6 nodes as PCN-222, a temperature of up to 573 K under vacuum was required to completely evacuate the porosity.[25] However, water adsorption isotherms described above

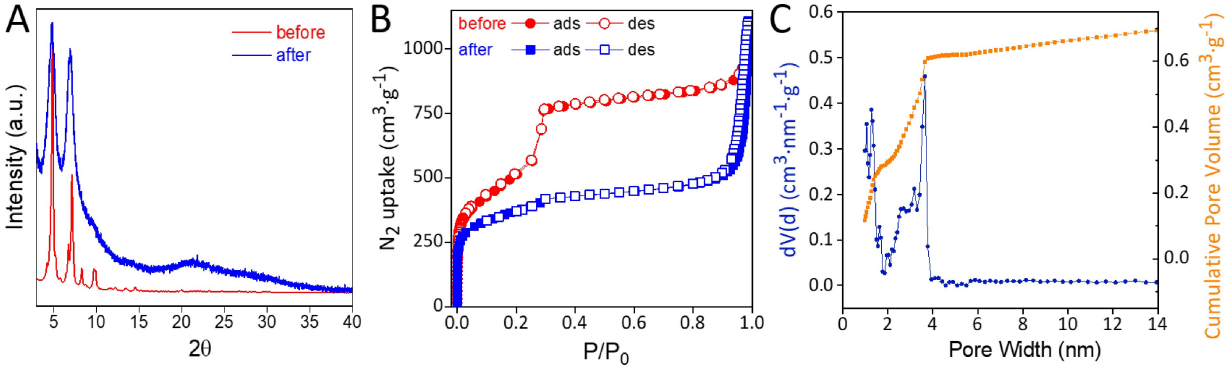

Figure 4. Characterization of the PCN-222 after the clathrates formation process: (A) PXRD pattern of PCN-222 after the clathrates formation, (B) N_2 isotherms and (C) the corresponding NLDFT pore size analysis. PXRD and isotherm of the PCN-222 as-synthesized (before) are also shown for easier comparison.

showed that H_2O can be easily removed from the inner cavities of the PCN-222 under ultra-high vacuum conditions and at 298 K, except the irreversible Zr_6-H_2O clusters. Residual H_2O molecules connected to the metallic clusters are present in minimal amounts and cannot explain the massive loss of mesoporosity. On the other hand, it is well known that under wet conditions (needed to promote the gas hydrate formation process) the D_2O molecules can strongly interact with the Zr metal clusters.[17] These adsorbate-framework interactions could weaken the rigidity and stability of the mesocavities (through the promotion of lattice defects, cluster disorders or linker vacancies). Furthermore, the application of a high-pressure stress in the pressure cell (high pressure hydrogen), and the volume expansion of confined D_2O from liquid to solid upon cooling (due to the lower density of solid D_2O), are likely sufficient to expect tremendous internal and external stresses in the PCN-222 network. Based on previous studies described in the literature by Bennett et al., under these demanding pressure conditions, we know that MOFs can experience amorphization to some extent, with the associated changes in the porous network.[26] An irreversible partial amorphization affecting mainly the mesoporous structure would lead to the observed results, i.e., the entrapment of D_2O molecules in a disordered morphology in the unidirectional channels of PCN-222 upon pressure (above 1.35 kbar), and the impossibility of these smaller pores to participate in further clathrate formation processes. The potential presence of some amorphous areas within the structure, with the consequent loss of the perfect crystallinity, could also explain the distorted ND pattern observed at 1.65 kPa and above, with a single peak at 3.6°, attributed to the (002) diffraction peak of disordered ice (vein-like). Notwithstanding, PCN-222 is also susceptible to experience a contraction of the mesoporous network (pore/volume shrinkage), while preserving the microporous structure, as inferred from the decline in the mesopore volume after the clathrate formation. Thus, at this stage, the two most likely scenarios of what happens to the PCN-222 material during the process would be: a partial amorphization of the structure or a framework shrinkage, both affecting mainly to the mesopores due to their higher flexibility and lower rigidity than micropores, while the latter remain practically unaffected. To shed more light into this complex process, recovered PCN-222 particles were examined by TEM (Figure S7). TEM images demonstrate the presence of important morphological changes in the recovered crystals, including the loss in the homogeneity of the original PCN-222 particles (Figure 1B), and surface corrugation and particle breakage. A detailed evaluation of an individual crystal provides conclusive proofs about the shrinkage of the mesoporous network (average pore size 1.8 nm), although the long-range ordering is slightly preserved, in agreement with the XRD discussed above. Interestingly, amorphization is also appreciable in certain regions. These observations allow to conclude that both, amorphization and framework shrinkage, are responsible for the structural changes observed in PCN-222 after the clathrate formation process. To identify the role of the high-pressure hydrogen in the aforementioned structural changes, as-synthesized PCN-222 was exposed to 1.8 kbar H_2 for 2 h at 298 K under dry conditions. XRD patterns (Figure S8) before and after high pressure exposure suggest that the structural deterioration in PCN-222 cannot be attributed to the instability of the material under high pressure conditions but rather to the instability during the clathrate formation/dissociation process, i.e., in the combined presence of D_2O and high pressure H_2.

Overall our findings show that mesoporous cavities in PCN-222 can act as nanoreactors to promote the nucleation and growth of hydrogen clathrate hydrates. Contrary to the generally accepted opinion in the literature regarding the preferential growth of gas hydrates outside the porosity, the ND data provide sufficient experimental evidences to suggest that these nucleation processes take place inside the mesocavities. In fact, these cavities in PCN-222 are large enough (pore diameter, 3.7 nm) to accommodate the crystal structure of the sII hydrate (crystal size, 1.7 nm). Unexpectedly, pressures above 1.35 kPa become detrimental for the proposed application due to the structural deterioration of PCN-222 (mainly affecting the mesoporous structure) as discussed above. Despite this limitation, this study constitutes the first experimental evidence about the potential role of MOFs as a host structure to promote hydrogen storage in the form of gas clathrate.

Conclusions

On the one hand, we have demonstrated that the synthesis of PCN-222 nanoparticles can be significantly improved using a MW-assisted method instead of the most common solvothermal methods, specifically in terms of faster kinetics, particles homogeneity, and better batch-to-batch reproducibility. The energy savings in the synthesis of MOFs by using the MW technology should also be seriously considered in view of the requirements imposed to move towards sustainable development. On the other hand, INS and ND measurements have demonstrated that mesopores in PCN-222 can be used as nanoreactors to promote the nucleation and growth of hydrogen clathrate crystals. These confined crystals can be grown at lower pressures than those used for bulk clathrate synthesis and with much faster kinetics. Despite the promising results achieved so far, the highly demanding pressure conditions under wet conditions needed for clathrate formation remain problematic due to their negative impact on the MOF structure (mainly on the mesoporous network). Nevertheless, considering the large structural versatility of MOFs, this study opens the gate to design new structures with the proper porous networks and surface functionalities needed to decrease the threshold pressure for the nucleation of these confined clathrates and with higher structural stability to prevent alterations of the MOF network during the complete formation/dissociation process, therefore enabling the reusability of the MOF for hydrogen storage.

Supporting Information

Full experimental procedures, characterization details, and additional supporting data and Figures. The authors have cited additional references within the Supporting Information (Ref. [27]).

Author Contributions

C.C.-C. designed and performed the synthesis of the PCN-222 nanoparticles, and completed their characterization; J.F.P. performed the adsorption experiments; L.D. and J.S.-A. performed the INS and ND measurements; Y.Q. and T.R.C. participated in the discussion of the INS and ND results; C.C.-C. and J.S.-A. participated in the preparation of the manuscript. All authors have reviewed the manuscript before submission.

Acknowledgements

Authors would like to acknowledge financial support from Ministerio de Ciencia e Innovación (Project PID2019-108453GB-C21 and PID2022-141034OB-C22), Consejo Superior de Investigaciones Científicas (CSIC) for internal funds (Intramural project, 202280I170), and Conselleria de Innovación, Universidades, Ciencia y Sociedad Digital (Project CIPROM/2021/022). A portion of this research used resources at the Spallation Neutron Source, a DOE Office of Science User Facility operated by the Oak Ridge National Laboratory (project IPTS-29742.1).

Conflict of Interest

The authors declare no conflict of interest.

Data Availability Statement

The data that support the findings of this study are available from the corresponding author upon reasonable request.

Keywords: Confinement Effects · Gas Hydrates · Hydrogen Storage · Metal–Organic Frameworks · Zirconium-Metalloporphyrin Framework

[1] E. D. Sloan, *Nature* **2003**, *426*, 353–359.
[2] W. L. Mao, H.-K. Mao, A. F. Goncharov, V. V. Struzhkin, Q. Guo, J. Hu, J. Shu, R. J. Hemley, M. Somayazulu, Y. Zhao, *Science* **2002**, *297*, 2247–2249.
[3] T. Collett, J. J. Bahk, R. Baker, R. Boswell, D. Divins, M. Frye, D. Goldberg, J. Husebo, C. Koh, M. Malone, M. Morell, G. Myers, C. Shipp, M. Torres, *J. Chem. Eng. Data* **2015**, *60*, 319–329.
[4] W. L. Vos, L. W. Finger, R. J. Hemley, H.-K. Mao, *Phys. Rev. Lett.* **1993**, *71*, 3150–3153.
[5] L. J. Florusse, C. J. Peters, J. Schoonman, K. C. Hester, C. A. Koh, S. F. Dec, K. N. Marsh, E. D. Sloan, *Science* **2004**, *306*, 469–471.
[6] H. Lee, J.-W. Lee, D. Y. Kim, J. Park, Y.-T. Seo, H. Zeng, I. L. Moudrakovski, C. I. Ratcliffe, J. A. Ripmeester, *Nature* **2005**, *434*, 743–746.
[7] J. Farrando-Perez, R. Balderas-Xicohtencatl, Y. Cheng, L. Daemen, C. Cuadrado-Collados, M. Martinez-Escandell, A. J. Ramirez-Cuesta, J. Silvestre-Albero, *Nat. Commun.* **2022**, *13*, 5953.
[8] L. Borchardt, W. Nickel, M. Casco, I. Senkovska, V. Bon, D. Wallacher, N. Grimm, S. Krause, J. Silvestre-Albero, *Phys. Chem. Chem. Phys.* **2016**, *18*, 20607–20614.
[9] M. E. Casco, F. Rey, J. L. Jordá, S. Rudic, F. Fauth, M. Martinez-Escandell, F. Rodriguez-Reinoso, E. V. Ramos-Fernández, J. Silvestre-Albero, *Chem. Sci.* **2016**, *7*, 3658–3666.
[10] D. Feng, Z. Y. Gu, J. R. Li, H. L. Jiang, Z. Wei, H. C. Zhou, *Angew. Chem. Int. Ed.* **2012**, *51*, 10307–10310.
[11] I. Thomas-Hillman, A. Laybourn, C. Dodds, S. W. Kingman, *J. Mater. Chem. A* **2018**, *6*, 11564–11581.
[12] N. A. Khan, S. H. Jhung, *Coord. Chem. Rev.* **2015**, *285*, 11–23.
[13] V. N. Le, H. T. Kwon, T. K. Vo, J.-H. Kim, W.-S. Kim, J. Kim, *Mater. Chem. Phys.* **2020**, *253*, 123278.
[14] X. Chen, Y. Zhuang, N. Rampal, R. Hewitt, G. Diviniti, C. A. O'Keefe, X. Liu, D. J. Whitaker, J. W. Wills, R. Jugdaohsingh, J. J. Powell, H. Yu, C. P. Grey, O. A. Scherman, D. Fairen-Jimenez, *J. Am. Chem. Soc.* **2021**, *143*, 13557–13572.
[15] K. S. W. Sing, *Pure Appl. Chem.* **1985**, *57*, 603–619.
[16] A. Grosman, C. Ortega, *Langmuir* **2005**, *21*, 10515–10521.
[17] B. Baumgartner, P. T. Prins, J. N. Louwen, M. Monai, B. M. Weckhuysen, *ChemCatChem* **2023**, *15*, e202300722.
[18] P. C. H. Mitchell, S. F. Parker, A. J. Ramirez-Cuesta, J. Tomkinson, *Vibrational Spectroscopy with Neutrons, in Series on Neutron Techniques and Applications: vol. 3*, World Scientific, Singapore, **2005**.
[19] T. L. Malkin, B. J. Murray, A. V. Brukhno, C. G. Salzmann, *Proc. Natl. Acad. Sci. USA* **2012**, *109*, 1041–1045.
[20] K. Morishige, H. Yasunaga, H. Uematsu, *J. Phys. Chem. C* **2009**, *113*, 3056–3061.
[21] H. L. B. Boström, S. Bette, S. T. Emmerling, M. W. Terban, B. V. Lotsch, *APL Mater.* **2022**, *10*, 071106.
[22] L. Peng, S. Yang, S. Jawahery, S. M. Moosavi, A. J. Huckaba, M. Asgari, E. Oveisi, M. K. Nazeeruddin, B. Smit, W. L. Queen, *J. Am. Chem. Soc.* **2019**, *141*, 12397–12405.
[23] I. E. Collings, A. L. Goodwin, *J. Appl. Phys.* **2019**, *126*, 181101.
[24] S. Henke, M. T. Wharmby, G. Kieslich, I. Hante, A. Schee-mann, Y. Wu, D. Daisenberger, A. K. Cheetham, *Chem. Sci.* **2018**, *9*, 1654–1660.
[25] J. E. Mondloch, M. J. Katz, W. C. Isley III, P. Ghosh, P. Liao, W. Bury, G. W. Wagner, M. G. Hall, J. B. DeCoste, G. W. Peterson, R. Q. Snurr, C. J. Cramer, J. T Hupp, O. K. Farha, *Nat. Mater.* **2015**, *14*, 512–516.
[26] T. D. Bennett, A. K. Cheetham, *Acc. Chem. Res.* **2014**, *47*, 1555–1562.
[27] H. Noh, C.-W. Kung, T. Islamoglu, A. W. Peters, Y. Liao, P. Li, S. J. Garibay, X. Zhang, M. R. DeStefano, J. T. Hupp, O. K. Farha, *Chem. Mater.* **2018**, *30*, 2193–2197.

Manuscript received: October 10, 2023
Accepted manuscript online: December 13, 2023
Version of record online: ■■, ■■

Research Articles

Metal-Organic Frameworks

C. Carrillo-Carrión,* J. Farrando-Perez, L. L. Daemen, Y. Q. Cheng, A. J. Ramirez-Cuesta, J. Silvestre-Albero* _ e202315280

Zr-Porphyrin Metal–Organic Framework as nanoreactor for boosting the formation of hydrogen clathrates

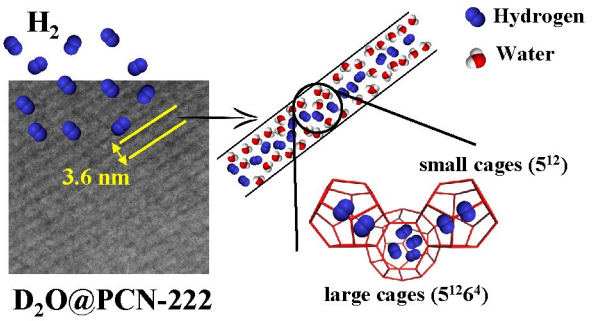

Microwave-assisted PCN-222 nanocrystals has been successfully used as nanoreactors to promote the nucleation and growth of hydrogen clathrates. This research shows that hydrogen can be enclathrated at lower pressure than the bulk system, with fast kinetics and with a nearly complete water-to-hydrate conversion.